IEEE Access
Multidisciplinary ⋮ Rapid Review ⋮ Open Access Journal

Received 31 January 2023, accepted 8 February 2023, date of publication 13 February 2023, date of current version 23 February 2023.

Digital Object Identifier 10.1109/ACCESS.2023.3244622

METHODS

Power Factor Correction Modulated Wireless Power Transfer System With Series-Series Compensation

WENXING ZHONG, (Senior Member, IEEE), SIJIA BAI, AND CHANGSHENG HU, (Senior Member, IEEE)
College of Electrical Engineering, Zhejiang University, Hangzhou, Zhejiang 310027, China

Corresponding author: Changsheng Hu (hucs@zju.edu.cn)

This work was supported by the National Natural Science Foundation of China under Grant 51807174.

ABSTRACT Power factor correction (PFC) is usually realized with a boost converter in a traditional power converter. This paper introduces a PFC modulated WPT method which can realize PFC function through phase-shift modulation of the primary-side inverter of a series-series (SS) WPT system. A close-loop control method of the phase-shift modulated system is also proposed for practical implementations. Without using a PFC converter, the structure of a WPT system can be simplified. Theoretical analysis and experimental results are provided to verify the idea.

INDEX TERMS Phase modulation, power factor correction, wireless power transfer.

I. INTRODUCTION

In recent years, energy and environmental problems have become increasingly serious, and the rise of electric vehicles (EVs) might be a solution to the pollution caused by the emissions of traditional fuel vehicles. As the scale of EVs continues to expand, it is urgent to solve the problems of insufficient supply of charging piles and unreasonable distribution of charging locations. Due to the emergence of high-power, high-switching frequency semiconductor devices, researches on WPT technology have been widely carried out. Compared with the traditional wired charging systems, WPT offers many benefits such as high electrical isolation, high flexibility and high reliability, especially in harsh environments. WPT has been widely adopted in transportation [1], [2], consumer electronics [3], [4], [5], [6], biomedical implantation [7], [8], [9], underwater equipment, energy hub [10], etc. In particular, it is of great significance for EV charging [11], [12], [13], [14], which can reduce battery storage requirements through opportunistic charging technology [15].

The associate editor coordinating the review of this manuscript and approving it for publication was Alon Kuperman.

Grid-connected power electronic converters need to limit the total harmonic distortion and have a high power factor. To reduce the grid reactive power and current harmonics, PFC converters are widely used in medium and high-power WPT systems. Active PFC circuits can be implemented using various converter topologies, including buck, boost, and flyback converters [16]. Among these topologies, boost converters are currently widely adopted (Fig. 1).

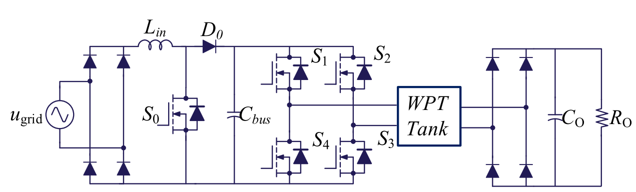

FIGURE 1. Traditional single-phase two-stage AC-DC WPT system with boost PFC.

According to the locations of the PFC converter, it can be divided into front-end PFC [17] and back-end PFC [18]. The classic front-end PFC is connected to the AC grid through a boost circuit to ensure high input power factor [19]. The front-end PFC converter of [20] consists of three parallel switches to reduce component stress and ensure safe

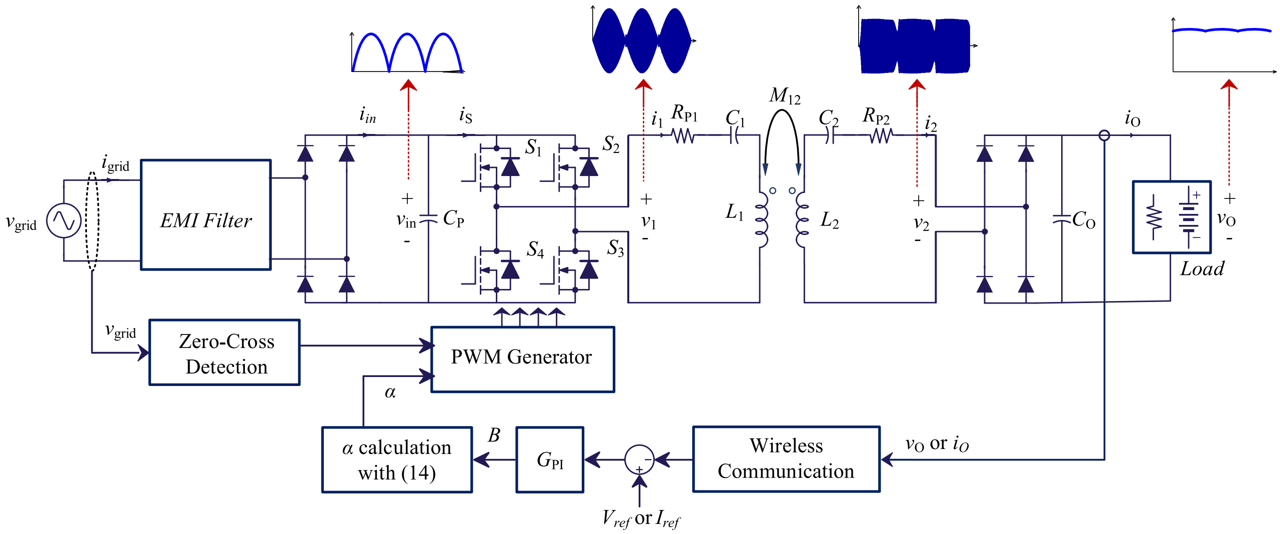

FIGURE 2. The WPT system with phase-shift PFC modulation.

operation of the circuit. The PFC converter is connected to the receiver in [21], and the topology is chosen so that the PFC stage has a sufficiently high input voltage with a weak coupling. The back-end PFC can simplify the structure of the primary side, but it will introduce pulsating power to the output [22].

Various approaches have been proposed to eliminate multiple stages in the transmitter of a WPT system. The commonly adopted technique is to use an AC-AC matrix converter to replace the traditional rectifier-PFC converter- inverter structure [23], [24]. Based on the series-parallel (SP) compensation topology, a three-phase AC-AC matrix converter comprising of six reverse-blocking switches and one regular switch, as long as a variable-frequency control strategy is proposed in [25] for WPT applications. PFC is realized by adopting the energy-injection and free-oscillation technique. A single-phase AC-AC matrix converter as well as an active rectifier are adopted in [26] to realize bidirectional WPT, based on dual-LCC compensation. The condition of realizing PFC have been derived and the modulation of secondary-side active rectifier is practically implemented. In [27], a current-fed AC-AC matrix converter with PFC function is proposed, which requires an energy storage inductor.

Apart from using a matrix converter, some other solutions are also reported to get rid of the PFC converter. In [28], frequency modulation is proposed for PFC with a rectifier-inverter and SP compensation topology. In [29], a single-stage WPT resonant converter with front-end bridgeless boost PFC rectifier is proposed. The bridgeless boost PFC converter is combined with the inverter so that less switches are required. In [30], a novel direct AC-AC converter is proposed for WPT systems. The converter only uses four regular switches for AC-AC conversation. However, the voltage usage rage of this converter is low and thereby it which performs AC-DC PFC rectification and DC-DC WPT conversion simultaneously to generate AC power containing line-frequency and high-frequency components. In [32], a T-type inverter is proposed for three-phase WPT system, which realizes PFC through duty cycle modulation, might be not suitable for high-power applications. In [31], only a full-bridge structure is designed on the primary side.

This paper proposes a PFC modulation method based on an SS WPT system. The grid voltage is directly supplied to the primary-side inverter after uncontrolled rectification. PFC function is realized through the phase-shift of the primary-side inverter. Compared with the traditional WPT system, this solution eliminates the PFC converter at the front-end of the primary inverter.

II. GENERAL ANALYSIS OF PFC MODULATION

The WPT system with the proposed PFC modulation is shown in Fig. 2. Compared with the traditional WPT system topology, the PFC circuit on the grid side is omitted, and the grid voltage is directly rectified into a 100 Hz pulsating voltage to supply the primary-side inverter of the WPT system. The operating frequency of the inverter is 85 kHz. To realize PFC, the only component to filter the 100 Hz pulsating power to DC power is the output capacitor C_O in this system. C_P is small for buffering the AC power in the switching frequency level. The output voltage amplitude of the inverter equals the grid pulsating voltage. V_{ref} and I_{ref} are the set reference values for the system output voltage and current. For this topology, the PFC function can be achieved only by primary-side modulation. The grid-side EMI filter filters out the 85 kHz high-frequency components.

The main idea of PFC in this system is to make the instantaneous output power of the inverter equal to the instantaneous input power from the grid as given by (3). To do so, phase-shift modulation of the inverter can be adopted, as shown in Fig.3.

Ideally, PFC means shaping the input current from the grid to be a sinusoidal wave which is in phase with the grid

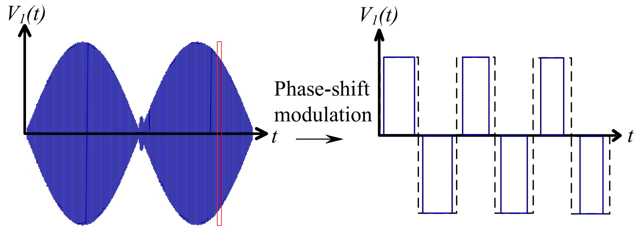

FIGURE 3. Inverter output voltage in one power frequency cycle, amplitude and duty cycle change with time.

voltage. Therefore, the input voltage and current are given by

$$v_{\text{grid}}(t) = \sqrt{2}V_{\text{grid}}\sin(\omega_0 t), \tag{1}$$

$$i_{\text{grid}}(t) = \sqrt{2}I_{\text{grid}}\sin(\omega_0 t), \tag{2}$$

where V_{grid} and I_{grid} are the RMS value of the grid voltage and current, respectively, and ω_0 is the angular frequency of the grid voltage. Then, the input power from the grid is given by

$$p_{\text{grid}}(t) = 2V_{\text{grid}}I_{\text{grid}}\sin^2(\omega_0 t). \tag{3}$$

The average input power is given by

$$P_{\text{grid}} = V_{\text{grid}}I_{\text{grid}}. \tag{4}$$

By neglecting the losses, the average input power P_{grid} of the system is equal to the average output power P_{O}, which is

$$P_{\text{grid}} = P_{\text{O}} = V_{\text{O}}I_{\text{O}}. \tag{5}$$

Then, the RMS value of the grid current is derived as

$$I_{\text{grid}} = \frac{V_{\text{O}}I_{\text{O}}}{V_{\text{grid}}}. \tag{6}$$

By substituting (6) into (3), (3) is rewritten as

$$p_{\text{grid}}(t) = 2V_{\text{O}}I_{\text{O}}\sin^2(\omega_0 t). \tag{7}$$

The circuit equations of the system are given by

$$\dot{V}_1 = (R_{\text{P1}} + jX_1)\dot{I}_1 + j\omega M\dot{I}_2, \tag{8}$$

$$\dot{V}_2 = j\omega M\dot{I}_1 + (R_{\text{P2}} + jX_2)\dot{I}_2, \tag{9}$$

where $X_{\text{i}} = \omega L_{\text{i}} - 1/(\omega C_{\text{i}})$, $i = 1, 2$, is the reactance of Resonator-i; M is the mutual inductance of coil L_1 and L_2; ω is the angular switching frequency of the inverter which is much higher than ω_0. Because C_{P} is a small capacitor which has negligible effect on the line-frequency power, the inverter output power is expected to be equal to the grid input power in the time scale of ω_0, i.e.

$$p_{\text{inv}}(t) = p_{\text{grid}}(t). \tag{10}$$

III. PFC WITH PHASE-SHIFT MODULATION

A. MODULATION SCHEME

Phase-shift modulation is widely adopted to regulate the output voltage of a full-bridge inverter by changing the relative phase angle between two inverter legs.

Firstly, also because C_{P} is a small capacitor which has negligible effect on the line-frequency voltage after rectification, the amplitude of the DC input voltage of the inverter is assumed the rectified grid voltage. In a switching cycle (or a half switching cycle), the input voltage of the inverter can be considered constant. Therefore, the RMS value of the fundamental component of the inverter output voltage in a switching cycle (or a half switching cycle) is given by

$$V_{1\_\text{inv}}(t) = \frac{2\sqrt{2}}{\pi}|\sqrt{2}\,V_{\text{grid}}\sin(\omega_0 t)|\sin\frac{\alpha}{2}, \tag{11}$$

where α is the phase-shift angle of the inverter, as shown in Fig. 4. It should be noted that V_{1_inv} is changing with the input voltage of the inverter (i.e., the rectified grid voltage).

In the WPT system in Fig. 1, the operating frequency f_{S} is equal to the resonant frequency f_{R} of two resonators, i.e., $X_1 = X_2 = 0$. The DC output voltage is constant, therefore, the RMS value of the fundamental component of the primary current i_1 can be derived with (9) by neglecting the effect of the parasitic resistance, which is

$$I_1 = \frac{2\sqrt{2}}{\pi}\frac{V_{\text{O}}}{\omega M}, \tag{12}$$

where V_{O} is the output voltage.

Because the input impedance of this system is pure resistive, the output power of the inverter is given by

$$p_{\text{inv\_inv}}(t) = |\sqrt{2}\,V_{\text{grid}}\sin\omega_0 t|\frac{8}{\pi^2}\frac{V_{\text{O}}}{\omega M}\sin\frac{\alpha}{2}. \tag{13}$$

By solving (10), the required phase-shift angle α is given by

$$\alpha = 2\arcsin(B|\sin\omega_0 t|), \tag{14}$$

where

$$B = \frac{\pi^2\omega M I_{\text{grid}}}{4\sqrt{2}\,V_{\text{O}}}, \text{ and } 0 < B < 1. \tag{15}$$

By substituting (6) into (15), B is rewritten as

$$B = \frac{\pi^2\omega M I_{\text{O}}}{4\sqrt{2}\,V_{\text{grid}}}, \text{ and } 0 < B < 1. \tag{16}$$

With (16), the AC equivalent resistance of the system R_{Le} is given by

$$R_{\text{Le}} = \frac{8}{\pi^2}\frac{V_O}{I_O} = \frac{\sqrt{2}\omega M V_{\text{O}}}{BV_{\text{grid}}}. \tag{17}$$

From (16), it can be seen that B is determined by the output current (I_{O}) provided that the other conditions are given. With a heavier load (i.e. larger I_{O}), a larger B is required. Fig. 5 shows the curves of α with different values of B from (14). The peak value of α increases with B. When $B = 1$, the peak value of α is π (rad), which means the inverter output voltage reaches the maximum at the time when the grid voltage peaks.

B. COUPLER DESIGN

The coupler design process of the phase-shift modulation system is provided in this section.

To maximize the usage rate of the input voltage of the inverter, B is set to 1 when designing the coupler. Firstly, the winding currents should be determined so that the number of strands of the wires can be determined. The primary winding current is calculated with (12) after the output voltage of the application is given. Similarly, the RMS value of the secondary winding current in the time scale of the inverter switching cycle can be estimated with

$$I_{2\_\mathrm{inv}}(t) = \frac{V_{1\_\mathrm{inv}}(t)}{\omega M}, \tag{18}$$

after the inverter output voltage is calculated with (11). This RMS value is changing with V_{1_inv} in double line frequency. To have the RMS value in the time scale of the line frequency, we can integrate it in a half line period

$$I_2 = \frac{1}{\pi}\int_0^{\pi} \frac{I_{2\_\mathrm{inv}}(\omega_0 t)}{\omega M} d(\omega_0 t). \tag{19}$$

Then the maximal mutual inductance for outputting the rated power is given by (16) and the optimal secondary winding inductance is given by [33] as

$$L_{2\_\mathrm{opt}} = \frac{8}{\pi^2}\frac{V_O}{k\omega I_O}. \tag{20}$$

Finally, the number of turns of the windings can be found with the help of finite-element simulations.

The efficiency of the system is given by [33]

$$\eta = \frac{I_2^2 R_{\mathrm{Le}}}{I_1^2 R_{\mathrm{P1}} + I_2^2 (R_{\mathrm{P2}} + R_{\mathrm{Le}})}, \tag{21}$$

where I_1 and I_2 are obtained from (12) and (19), R_{Le} is obtained from (17).

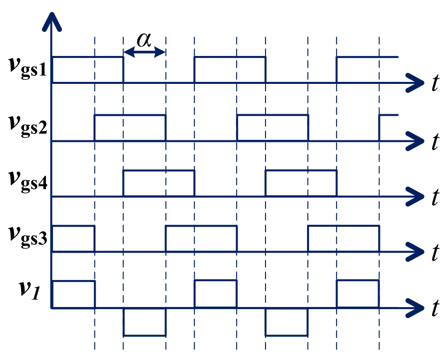

FIGURE 4. Phase shift angle of the inverter.

C. SIMULATION VERIFICATION

Simulation studies have been carried out with parameters given in Table 1. A three-stage compound EMI filter is used in experiments. The structure and parameters of the same filter

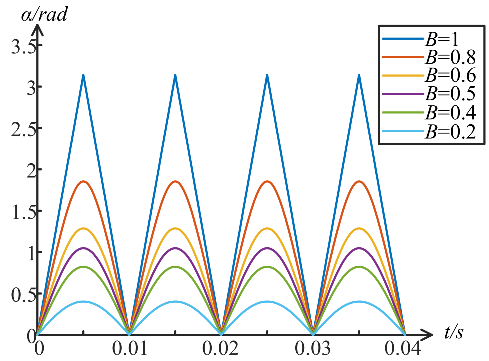

FIGURE 5. Curves of α with different values of B.

TABLE 1. WPT system parameters.

Parameter	Value	Parameter	Value
Grid voltage, V_{grid}	220 V	Filter capacitor, C_{O}	8 mF
Line frequency, f	50 Hz	Load resistance, R_{L}	5 Ω
Filter capacitor, C_{P}	5.00 uF	M_{12}	9.07 uH
L_1	52.68 uH	L_2	31.97 uH
Wire of primary coil	0.1 mm× 1200strands	Wire of secondary coil	0.1 mm× 1500strands
N_1	9	N_2	7
C_1	66.29 nF	C_2	109.6 nF
R_{P1}	0.197 Ω	R_{P2}	0.236 Ω

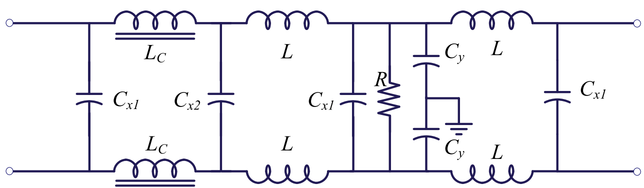

FIGURE 6. The EMI filter used in the simulations and experiments.

TABLE 2. EMI filter parameters.

Parameters	Numerical value
L_C	0.8mH
L	0.3mH
C_{x1}	0.1uF
C_{x2}	1nF
C_y	3.3uF
R	1MΩ

are used in the simulations, as shown in Fig. 6 and Table 2, respectively.

Table 3 shows the simulation results with different values of B. The load resistance varies widely and the system maintains constant voltage output. As long as the output voltage and output power are given, the required B can be calculated with (16). However, it is difficult to obtain the accurate value of the mutual inductance needed in (16). Alternatively, B can be considered as a control variable which is determined by a negative-feedback controller such as the proportional-integral (PI) controller in a close-loop manner. Then as long as the phase-shift angle of the inverter follows (14), PFC is realized.

TABLE 3. Impact of *B* on system performance.

R_L	B	Grid current	Inverter output voltage, V_1	Zoomed views of inverter output voltage at peak	Output voltage, V_O	Output power, P_O
20Ω	0.28	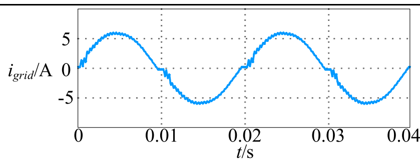	84.3V	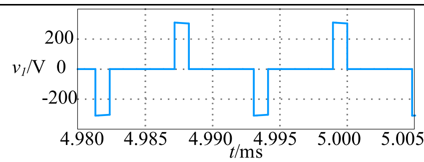	122.1V	745.4W
12Ω	0.44	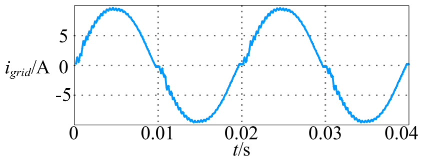	106.5V	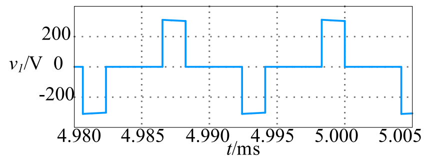	121.9V	1238.3W
8Ω	0.64	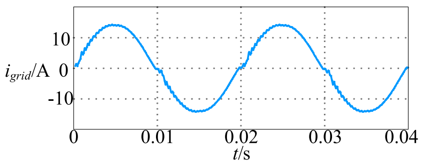	130.6V	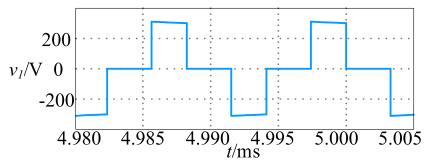	121.9V	1857.5W
6Ω	0.84	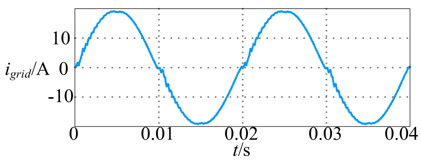	154.4V	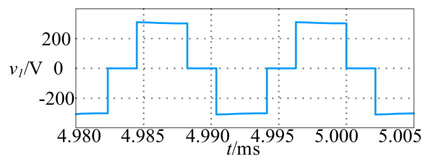	121.9V	2476.7W
5Ω	1	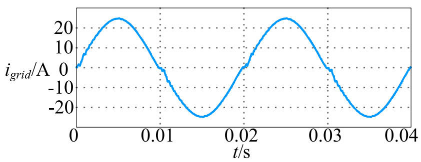	180.1V	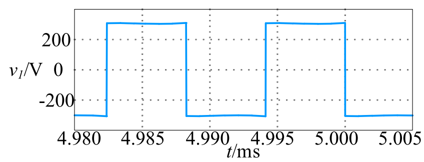	121.9V	2971.9W

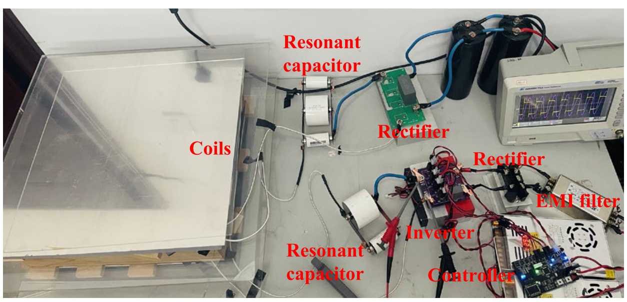

FIGURE 7. Experiment platform of the PFC modulated WPT system.

IV. EXPERIMENTAL VERIFICATION

A 3.3 kW prototype is built for experiments, based on the WPT system topology given in Fig. 2. The size of the primary and secondary coils is 400mm×400mm, and the air gap is 150mm. The primary circuit includes an input EMI filter, a full-bridge rectifier, and a full-bridge inverter constructed with SiC MOSFET C2M0025120D from CREE. The secondary side adopts an uncontrolled rectifier. The system parameters are given in Table 1 and the experiment platform is shown in Fig. 7.

The performances of the system with PFC modulation method are given in Fig 8-16. Fig. 8 shows the grid voltage and current waveforms of phase-shift modulation method. The grid current follows the grid voltage very well. Fig. 9 and 10 shows the inverter output voltage and current waveforms for phase-shift modulation with $B = 1$ and $B = 0.5$, respectively. The inverter output voltage is modulated with the phase-shift angles given by (14) and the inverter output current maintains constant which is determined by (12) at most of the time expect for the zero- crossing region. Fig. 11 and 12 shows secondary-side rectifier input voltage and current waveforms for phase-shift modulation. Moreover, it is clear that the output of the phase-shift modulated system can be regulated by changing B. A closed-loop control of the phase-shift modulated system is illustrated in Fig. 13. By regulating B in a close-loop manner, the output voltage of the system slowly increases from zero to the desired value. The output voltage ripple is 4.07 V. The changes of the inverter output voltage and current are shown in Fig. 14. As predicted by the analysis, the duty cycle of the inverter output voltage gradually increases with B. Fig. 15 and 16 shows the measured results when there is a step change in load power. The output of the system can be regulated to follow

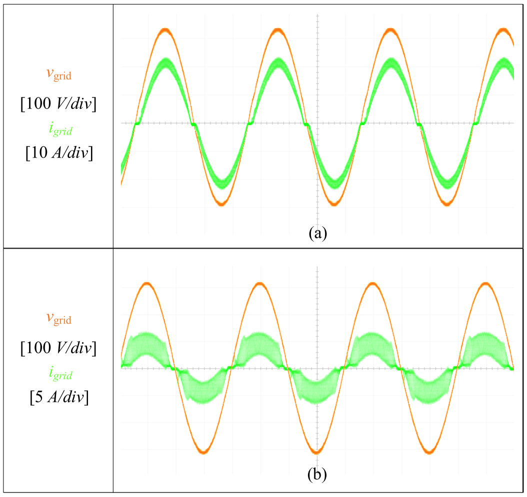

FIGURE 8. Phase-shift modulation: grid voltage and current waveforms: (a) B=1, (b) B=0.5.

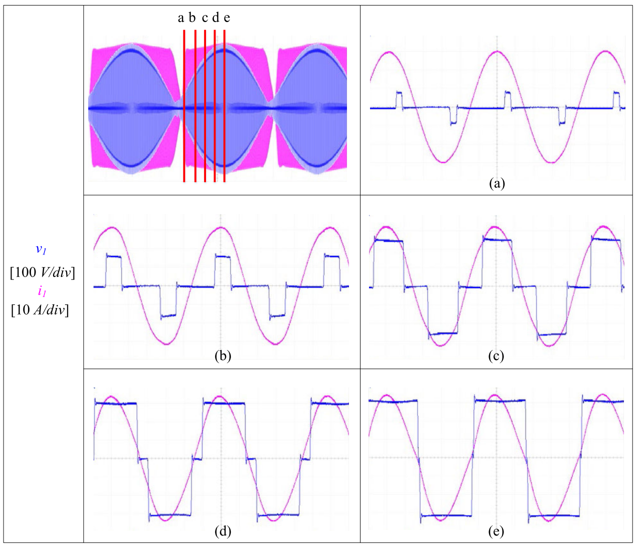

FIGURE 9. Phase-shift modulation (B=1): inverter output voltage and current waveforms. (a), (b), (c), (d), (e) Zoomed views at different moments.

TABLE 4. Experimental results.

	Phase-shift modulation (B=1)	Phase-shift modulation (B=0.5)
PF of grid voltage and current, λ_{grid}	0.999	0.999
Grid power, P_{grid}	3144 W	682 W
Output voltage, V_O	120 V	54 V
Output current, I_O	24A	10.8A
Output power, P_O	2880 W	583 W
System efficiency, η	91.6%	85.48%

the reference through closed-loop control after the load change.

Table 4 gives the measured power factor and efficiency. It is obvious that the output voltage of the phase-shift modulated system is proportional to B if the load resistance is unchanged.

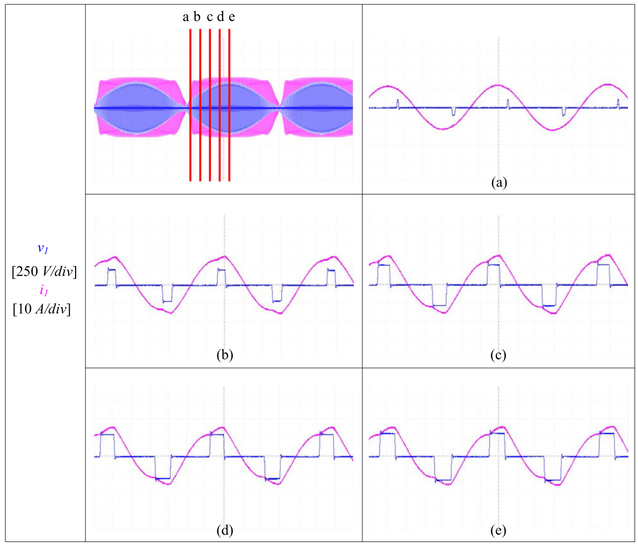

FIGURE 10. Phase-shift modulation (B=0.5): inverter output voltage and current waveforms. (a),(b),(c),(d),(e) Zoomed views at different moments.

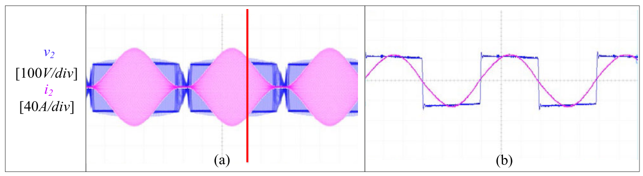

FIGURE 11. Phase-shift modulation (B=1): secondary-side rectifier input voltage and current waveforms. (a) over view, (b) zoomed views.

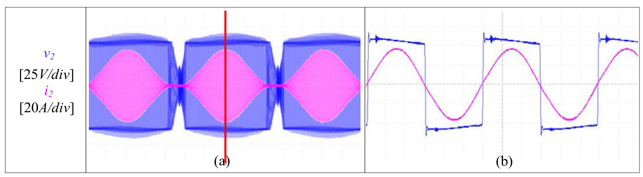

FIGURE 12. Phase-shift modulation (B=0.5): secondary-side rectifier input voltage and current waveforms. (a) over view, (b) zoomed views.

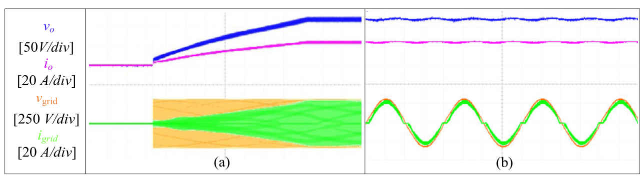

FIGURE 13. Close loop operation of the phase-shift modulated system: (a) changes of the grid voltage and current, system output voltage and current at the start-up stage, (b) zoomed views at the steady stage.

The efficiency of $B = 0.5$ is lower than that of $B = 1$. There are two main reasons. First, $B = 0.5$ has higher switching losses. Referring to Fig. 9 (e) and Fig. 10 (e), when $B = 1$, the zero-crossing points of the inverter output voltage and the inverter output current are closed and thereby, the switching losses are low; when $B = 0.5$, the duty cycle of the inverter voltage is much lower which leads to larger

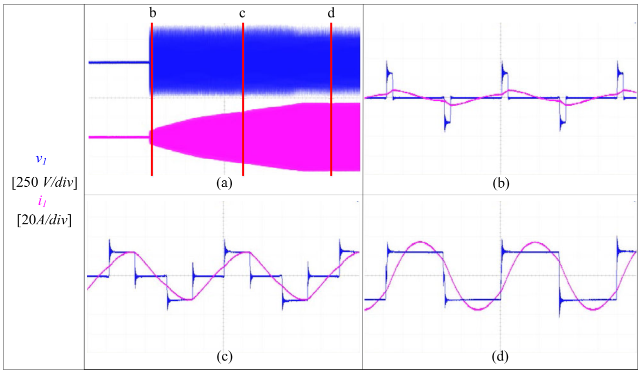

FIGURE 14. Inverter output voltage and current waveforms at the start-up stage of the phase-shift modulated system: (a) over view, (b) (c) and (d) zoomed views at different positions.

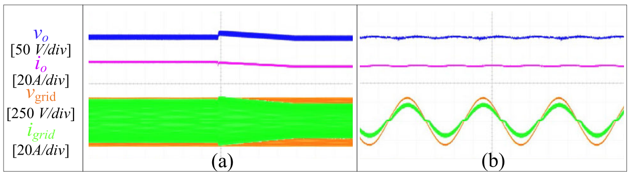

FIGURE 15. Close loop operation of the phase-shift modulated system with a step change in load power: (a) changes of the grid voltage and current, system output voltage and current at the start-up stage, (b) zoomed views at the steady stage.

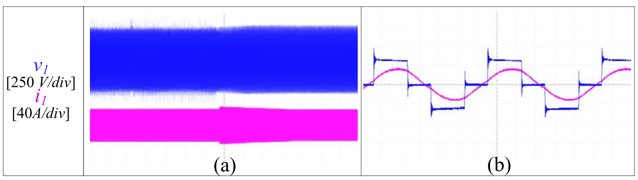

FIGURE 16. Inverter output voltage and current waveforms of the phase-shift modulated system with a step change in load power: (a) over view, (b) zoomed views at the steady stage.

TABLE 5. The ODD harmonics of grid current.

Harmonic order	Maximum allowable harmonic current		
	Standard value	Phase-shift modulation (B=1)	Phase-shift modulation (B=0.5)
3	2.30 A	0.982 A	0.194 A
5	1.14 A	0.470 A	0.107 A
7	0.77 A	0.430 A	0.070 A
9	0.40 A	0.264 A	0.042 A
11	0.33 A	0.186 A	0.022 A
13	0.21 A	0.092 A	0.020 A

turn-on and also turn-off losses. It should be noted that the switching losses in the time period when the grid voltage is closed to the peak is dominant because the inverter DC voltage is higher. Second, when $B = 0.5$, the output current is lower, which makes the equivalent resistance of the diode rectifier larger. In other words, the percentage of the rectifier loss will become higher. Table 5 gives measured harmonics of the system with phase-shift modulation. The power factor and harmonics comply with the standard requirements [34] well.

V. CONCLUSION

This paper proposes a PFC-modulated WPT system which realizes PFC function through the phase-shift modulation of the primary-side inverter of the WPT system. Thereby, no PFC converter is required. The required phase-shift angle of the inverter is calculated. Experimental results verify that the WPT system can realize PFC through the proposed modulation method. Close loop control for the phase-shift PFC modulation is introduced.

REFERENCES

[1] S. Lee, B. Choi, and C. T. Rim, "Dynamics characterization of the inductive power transfer system for online electric vehicles by Laplace phasor transform," *IEEE Trans. Power Electron.*, vol. 28, no. 12, pp. 5902–5909, Dec. 2013.

[2] G. A. Covic and J. T. Boys, "Modern trends in inductive power transfer for transportation applications," *IEEE J. Emerg. Sel. Topics Power Electron.*, vol. 1, no. 1, pp. 28–41, Mar. 2013.

[3] S. Y. R. Hui and W. W. C. Ho, "A new generation of universal contactless battery charging platform for portable consumer electronic equipment," *IEEE Trans. Power Electron.*, vol. 20, no. 3, pp. 620–627, May 2005.

[4] V. T. Nguyen, S. H. Kang, J. H. Choi, and C. W. Jung, "Magnetic resonance wireless power transfer using three-coil system with single planar receiver for laptop applications," *IEEE Trans. Consum. Electron.*, vol. 61, no. 2, pp. 160–166, May 2015.

[5] A. P. Sample, B. H. Waters, S. T. Wisdom, and J. R. Smith, "Enabling seamless wireless power delivery in dynamic environments," *Proc. IEEE*, vol. 101, no. 6, pp. 1343–1358, Jun. 2013.

[6] S. M. Rakiul Islam, S. Maxwell, M. K. Hossain, S.-Y. Park, and S. Park, "Reactive power distribution strategy using power factor correction converters for smart home application," in *Proc. IEEE Energy Convers. Congr. Expo. (ECCE)*, Sep. 2016, pp. 1–6.

[7] D. Ahn and S. Hong, "Wireless power transmission with self-regulated output voltage for biomedical implant," *IEEE Trans. Ind. Electron.*, vol. 61, no. 5, pp. 2225–2235, May 2014.

[8] P. Si, A. P. Hu, S. Malpas, and D. Budgett, "A frequency control method for regulating wireless power to implantable devices," *IEEE Trans. Biomed. Circuits Syst.*, vol. 2, no. 1, pp. 22–29, Mar. 2008.

[9] G. Wang, W. Liu, M. Sivaprakasam, and G. A. Kendir, "Design and analysis of an adaptive transcutaneous power telemetry for biomedical implants," *IEEE Trans. Circuits Syst. I, Reg. Papers*, vol. 52, no. 10, pp. 2109–2117, Oct. 2005.

[10] M. Kim, H. Park, and J. Jung, "Wireless power transfer converter for energy hub applications with high power factor capability," in *Proc. IEEE 3rd Int. Future Energy Electron. Conf. ECCE Asia (IFEEC ECCE Asia)*, Jun. 2017, pp. 643–647.

[11] A. Burkert and B. Schmuelling, "Comparison of two power factor correction topologies on conducted emissions in wireless power transfer systems for electric vehicles," in *Proc. IEEE Vehicle Power Propuls. Conf. (VPPC)*, Oct. 2021, pp. 1–6.

[12] C. Lu, Z. Guo, W. Qu, W. Wang, X. Yu, and X. Liu, "Design of PFC in wireless charging system for electric vehicle," in *Proc. 2nd IEEE Conf. Energy Internet Energy Syst. Integr. (EI)*, Oct. 2018, pp. 1–5.

[13] L. Tang, M. Chinthavali, O. C. Onar, S. Campbell, and J. M. Miller, "SiC MOSFET based single phase active boost rectifier with power factor correction for wireless power transfer applications," in *Proc. IEEE Appl. Power Electron. Conf. Expo. (APEC)*, Mar. 2014, pp. 3258–3265.

[14] O. C. Onar, M. Chinthavali, S. L. Campbell, L. E. Seiber, and C. P. White, "Vehicular integration of wireless power transfer systems and hardware interoperability case studies," *IEEE Trans. Ind. Appl.*, vol. 55, no. 5, pp. 5223–5234, Sep. 2019.

[15] F. Musavi and W. Eberle, "Overview of wireless power transfer technologies for electric vehicle battery charging," *IET Power Electron.*, vol. 7, no. 1, pp. 60–66, Jan. 2014.

[16] H.-T. Cho, J. Kim, J. Jung, and K. A. Kim, "Comparison of input power factor correction techniques for buck converters in single-phase wireless power transfer systems," in *Proc. IEEE PELS Workshop Emerg. Technolog., Wireless Power (WoW)*, Jun. 2015, pp. 1–8.

[17] M. Chinthavali, O. C. Onar, S. L. Campbell, and L. M. Tolbert, "Integrated charger with wireless charging and boost functions for PHEV and EV applications," in *Proc. IEEE Transp. Electrific. Conf. Expo. (ITEC)*, Jun. 2015, pp. 1–8.

[18] J. E. Huber, D. Rothmund, L. Wang, and J. W. Kolar, "Full-ZVS modulation for all-SiC ISOP-type isolated front end (IFE) solid-state transformer," in *Proc. IEEE Energy Convers. Congr. Expo. (ECCE)*, Sep. 2016, pp. 1–8.

[19] Y. Guo, L. Wang, C. Tao, C. Liao, and Q. Zhu, "Analysis of power factor correction circuit for EV wireless charging system," in *Proc. IEEE Conf. Expo. Transp. Electrific. Asia–Pacific (ITEC Asia–Pacific)*, Aug. 2014, pp. 1–5.

[20] S. Rahman, Y. Kosesoy, M. A. Ozdemir, O. Simsek, M. T. Aydemir, and A. Chub, "Design and practical implementation of a parallel-switched power factor correction boost converter," in *Proc. 14th IEEE Int. Conf. Ind. Appl. (INDUSCON)*, Aug. 2021, pp. 395–400.

[21] J. M. Arteaga, S. Aldhaher, D. C. Yates, and P. D. Mitcheson, "A multi-MHz wireless power transfer system with mains power factor correction circuitry on the receiver," in *Proc. IEEE Appl. Power Electron. Conf. Expo. (APEC)*, Mar. 2019, pp. 683–688.

[22] A. Avila, A. Garcia-Bediaga, U. Iruretagoyena, I. Villar, and A. Rujas, "Comparative evaluation of front- and back-end PFC IPT systems for a contactless battery charger," *IEEE Trans. Ind. Appl.*, vol. 54, no. 5, pp. 4842–4850, Sep. 2018.

[23] A. Ecklebe, A. Lindemann, and S. Schulz, "Bidirectional switch commutation for a matrix converter supplying a series resonant load," *IEEE Trans. Power Electron.*, vol. 24, no. 5, pp. 1173–1181, May 2009.

[24] N. X. Bac, D. M. Vilathgamuwa, and U. K. Madawala, "A SiC-based matrix converter topology for inductive power transfer system," *IEEE Trans. Power Electron.*, vol. 29, no. 8, pp. 4029–4038, Aug. 2014.

[25] M. Moghaddami, A. Anzalchi, and A. I. Sarwat, "Single-stage three-phase AC-AC matrix converter for inductive power transfer systems," *IEEE Trans. Ind. Electron.*, vol. 63, no. 10, pp. 6613–6622, Oct. 2016.

[26] S. Weerasinghe, U. K. Madawala, and D. J. Thrimawithana, "A matrix converter-based bidirectional contactless grid interface," *IEEE Trans. Power Electron.*, vol. 32, no. 3, pp. 1755–1766, Mar. 2017.

[27] S. Samanta and A. K. Rathore, "A new inductive power transfer topology using direct AC-AC converter with active source current waveshaping," *IEEE Trans. Power Electron.*, vol. 33, no. 7, pp. 5565–5577, Jul. 2018.

[28] M. G. Egan, D. L. O'Sullivan, J. G. Hayes, M. J. Willers, and C. P. Henze, "Power-factor-corrected single-stage inductive charger for electric vehicle batteries," *IEEE Trans. Ind. Electron.*, vol. 54, no. 2, pp. 1217–1226, Apr. 2007.

[29] J. Liu, K. W. Chan, C. Y. Chung, N. H. L. Chan, M. Liu, and W. Xu, "Single-stage wireless-power-transfer resonant converter with boost bridgeless power-factor-correction rectifier," *IEEE Trans. Ind. Electron.*, vol. 65, no. 3, pp. 2145–2155, Mar. 2018.

[30] H. L. Li, A. P. Hu, and G. A. Covic, "A direct AC–AC converter for inductive power-transfer systems," *IEEE Trans. Power Electron.*, vol. 27, no. 2, pp. 661–668, Feb. 2012.

[31] J. Liu, F. Xu, C. Sun, and K. H. Loo, "A compact single-phase AC–DC wireless power transfer converter with active power factor correction," *IEEE Trans. Ind. Electron.*, vol. 70, no. 4, pp. 3685–3696, Apr. 2023.

[32] J. Liu, W. Xu, K. W. Chan, M. Liu, X. Zhang, and N. H. L. Chan, "A three-phase single-stage AC–DC wireless-power-transfer converter with power factor correction and bus voltage control," *IEEE J. Emerg. Sel. Topics Power Electron.*, vol. 8, no. 2, pp. 1782–1800, Jun. 2020.

[33] J. Mühlethaler, "Modeling and multi-objective optimization of inductive power components," Ph.D. dissertation, Dept. Inf. Technol. Elect. Eng., ETH Zurich, Zürich, Switzerland, 2012.

[34] *Electromagnetic Compatibility (EMC)—Part 3–2: Limits Limits for Harmonic Current Emissions (Equipment Input Current ≤16 A Per Phase)*, document IEC 61000-3-2, 2018.

WENXING ZHONG (Senior Member, IEEE) received the B.Eng. degree in electrical engineering from Tsinghua University, China, in 2007, and the Ph.D. degree from the City University of Hong Kong, Hong Kong, in 2012. From March 2016 to May 2017, he was a Research Assistant Professor at the Department of Electrical and Electronic Engineering, The University of Hong Kong, Hong Kong. Currently, he is a Professor with the Department of Electrical Engineering, Zhejiang University, China. His research interests include wireless power transfer and power electronics. He received the two Transactions First Prize Paper Awards from the IEEE Power Electronics Society.

SIJIA BAI received the B.Eng. degree from the Hangzhou Dianzi University, Hangzhou, China, in 2020. She is currently pursuing the M.Sc. degree with the Department of Electrical Engineering, Zhejiang University, Hangzhou.

Her research interest includes wireless power transfer technologies.

CHANGSHENG HU (Senior Member, IEEE) received the bachelor's degree in motor and controls and the master's degree in power electronics from the Hefei University of Technology, in 1995 and 1998, respectively, and the Ph.D. degree in power electronics from Zhejiang University, China, in 2002.

He is an Associate Professor with the Department of Applied Electronic. He has engaged in power conversion technology and electromagnetic compatibility technology. His research interests include the energy conversion and energy efficiency applications, such as converter for EV and charging stations, renewable energy grid integration, energy-storage unit, modeling, and suppression technology of EMI.